Fatigue of Steel

Constant-Amplitude Load on CCT-Specimens

Gansted, L.

Publication date:
1993

Document Version
Early version, also known as pre-print

INSTITUTTET FOR BYGNINGSTEKNIK
DEPT. OF BUILDING TECHNOLOGY AND STRUCTURAL ENGINEERING
AALBORG UNIVERSITETSCENTER • AUC • AALBORG • DANMARK

FRACTURE & DYNAMICS
PAPER NO. 49

L. GANSTED
FATIGUE OF STEEL:
CONSTANT-AMPLITUDE LOAD ON CCT-SPECIMENS

DECEMBER 1993 ISSN 0902-7513 R9344

The FRACTURE AND DYNAMICS papers are issued for early dissemination of research results from the Structural Fracture and Dynamics Group at the Department of Building Technology and Structural Engineering, University of Aalborg. These papers are generally submitted to scientific meetings, conferences or journals and should therefore not be widely distributed. Whenever possible reference should be given to the final publications (proceedings, journals, etc.) and not to the Fracture and Dynamics papers.

INSTITUTTET FOR BYGNINGSTEKNIK
DEPT. OF BUILDING TECHNOLOGY AND STRUCTURAL ENGINEERING
AALBORG UNIVERSITETSCENTER • AUC • AALBORG • DANMARK

FRACTURE & DYNAMICS
PAPER NO. 49

L. GANSTED
FATIGUE OF STEEL:
CONSTANT-AMPLITUDE LOAD ON CCT-SPECIMENS
DECEMBER 1993 ISSN 0902-7513 R9344

Fatigue of Steel: Constant-Amplitude Load on CCT-Specimens

Lise Gansted
University of Aalborg
Sohngaardsholmsvej 57
DK-9000 Aalborg
Denmark

ABSTRACT

Based on the still increasing problems concerning fatigue failures in civil engineering structures, the fatigue properties of mild steel are determined in this paper. Three test series have been performed, one with static load and two with deterministic, constant-amplitude load. Hereby, the SN-curve and the statistical properties of the fatigue crack growth data are found.

KEYWORDS

Mild steel, centre-cracked-tension-specimens (CCT-specimens), material properties, constant-amplitude load, SN-curve, fatigue crack growth data.

1. INTRODUCTION

Since many civil engineering structures are influenced by time-varying load and since the structures are increased in size and slenderness, more and more structures are becoming sensitive to fatigue. Thus, it is important to obtain knowledge on the properties of fatigue in materials used for civil engineering structures and take this knowledge into account in the design of structures.

The present paper describes three series of tests performed on mild steel. The chemical composition is given in table 1.1.

Ec	C	Si	Mn	P	S	N	Cr	Ni	Cu	Al
0.14	0.07	0.01	0.33	0.012	0.009	0.004	0.04	0.03	0.01	0.038

Table 1.1: Chemical composition of the STW22 DIN 1614 steel used in experimental tests. In percentage by weight.

The first test series has been performed with static load in order to determine the

material parameters, i.e. the modulus of elasticity E, the Poisson ratio ν, the yield stress f_y the ultimate stess f_u and the ultimate strain ϵ_u of mild steel. The static tests are described in chapter 2.

The second and third series of tests have been performed with time-varying load with constant amplitude (CA-load) in order to establish the fatigue properties of mild steel given in table 1.1. The series described in section 3.1 includes different stress ranges, whereas the series described in section 3.2 only includes one stress range chosen on the basis of the results in section 3.1.

Besides determination of the properties of fatigue the tests serve as reference data in the test of the FMF-model described in [Gansted, L., R. Brincker and L. Pilegaard Hansen; 1991] and [Gansted, L., R. Brincker and L. Pilegaard Hansen; 1994].

Finally, the statistical properties of the fatigue data from the third test series are given in section 3.3.

2. STATIC TESTS

The purpose of the static tests described in this chapter is to determine the modulus of elasticity E, the Poisson ratio ν, the yield stress f_y the ultimate stress f_u and the ultimate strain ϵ_u.

Two test specimens, shown in figure 2.1, are carved from the same steel cast as the one used in the fatigue tests described in chapter 3. One rosette strain gauge (3 measuring grids) and two single strain gauges (1 measuring grid), all with the resistance 120 Ω, are stuck on each side of the specimens, see figure 2.1.

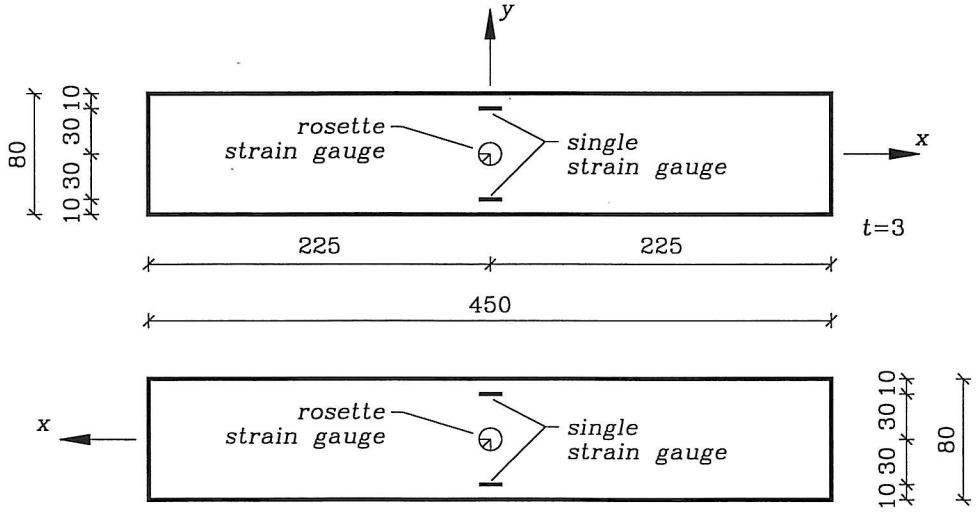

Figure 2.1: Dimensions of the test specimen, position of the strain gauges and statement of the coordinate system.
All measurements in mm.

The test specimen are placed in a tension/compression test machine of the type "Mohr-Federhaff" and the strain measurements are performed with a "Brüel & Kjær Strain Indicator Type 1526". The strain gauges are coherent in a Wheatstone bridge with one active gauge (quarter bridge).

Assuming uniaxial stress field, the Poisson ratio is given as

$$\nu = -\frac{\epsilon_y}{\epsilon_x} \tag{2.1}$$

and the modulus of elasticity as

$$E = \frac{\sigma_x}{\epsilon_x} = \frac{P_x}{b\ t\ \epsilon_x} \tag{2.2}$$

where

ϵ_x = strain in the x-direction
ϵ_y = strain in the y-direction
σ_x = normal stress in the x-direction [MPa]
P_x = applied load in the x-direction [MPa]
b = width of the test specimen [mm]
t = thickness of the test specimen [mm]

Compensation for the possible skewness in the load and in the position of the strain gauges is sought by using the mean values of the strain in symmetrically placed gauges.

The Poisson ratio and the modulus of elasticity are found by linear regression analysis of ϵ_y as a function of ϵ_x and σ_x as a function of ϵ_x, respectively. The results are given in table 2.3.

The stress-strain relation is determined by using a test specimen with width w and thickness t, $w \cdot t = 99.9 \cdot 2.8$ mm^2, and with the length $l_0 = 450$ mm.

The specimen is placed in the "Mohr-Federhaff" tension/compression test machine so the specimen is loaded in the direction of the length. The distance between the strengthening clamps is recorded before loading. The displacement transducer and the load cell in the test machine are connected to a x-y-plotter ("Kipp & Zonen") so the coherent values of the displacement u between the strengthening clamps and the applied load P are registered.

The load is increased from zero until fracture. Unloading and re-loading at initial yielding may be performed. The ultimate load P_u is read and the deformed length l_u of the specimen is measured.

From the stress-strain relation the yield stress is found as

$$f_y = \frac{P_y}{b\ t} \tag{2.3}$$

the ultimate stress as

$$f_u = \frac{P_u}{b\,t} \tag{2.4}$$

and the ultimate strain as

$$\epsilon_u = \frac{l_u - l_0}{l_i} \tag{2.5}$$

where

$P_y =$ load at which yielding takes place [N]
$P_u =$ load at which fracture takes place [N]
$l_u =$ deformed length [mm]
$l_0 =$ undeformed length [mm]
$l_i =$ initial length between the strengthening clamps [mm]

The parameters used to calculate the material parameters are given in table 2.2, whereas all the material parameters are given in table 2.3.

w [mm]	t [mm]	l_0 [mm]	l_i [mm]	l_u [mm]	P_y [10^3 N]	P_u [10^3 N]
99.9	2.8	450	275	527	74.4	92.4

Table 2.2: Parameters used to calculate the material properties for mild steel given in table 1.1.

According to (2.1)-(2.5), the material parameters are

Modulus of elasticity E	$1.9 \cdot 10^5$ MPa
Poisson ratio ν	0.28
Yield stress f_y	266 MPa
Ultimate stress f_u	330 MPa
Ultimate strain ϵ_u	0.28

Table 2.3: Material properties for mild steel given in table 1.1.

3. FATIGUE TESTS

As mentioned in chapter 1, two series of fatigue tests with CA-load have been performed in order to establish the fatigue properties of mild steel given in table 1.1.

The series described in section 3.1 includes different stress ranges, whereas the series described in section 3.2 are performed under "identical" conditions.

The specimens, which were carved from the same steel plate, were arbitrarily chosen for the two test series. In all the fatigue tests, CCT-specimens (Centre Cracked Tension Specimen) have been used, see figure 3.1.

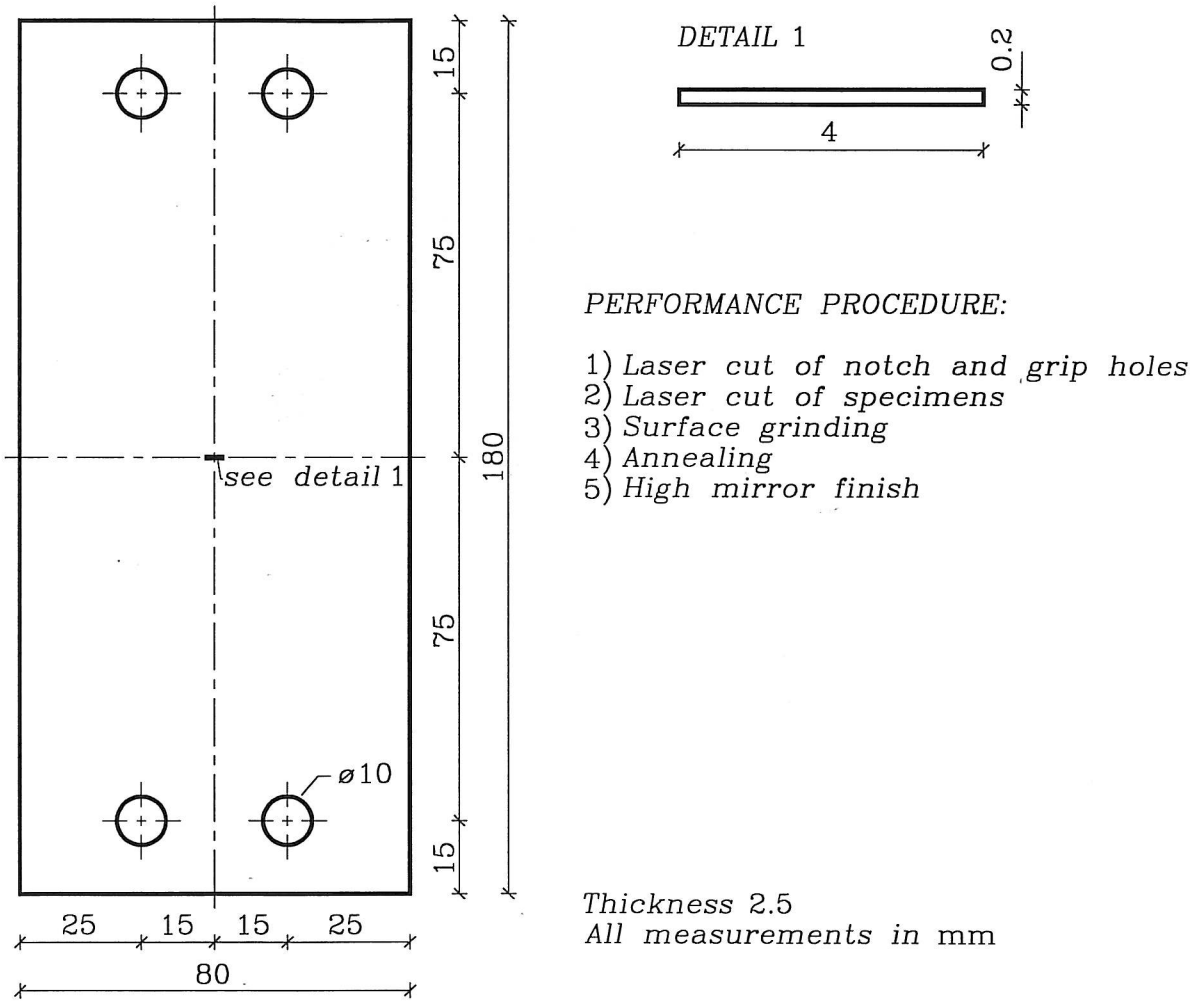

Figure 3.1: CCT-specimen used in fatigue testing.

The test equipment shown in figure 3.2 consists of a servo-hydraulic fatigue testing machine (± 40 kN), a camera including a monitor and a PC used as controller. The PC is equipped with image analysing hardware (cards) used in Digital Image Processing (DIP). The software control program consists of two parts, one used to control the fatigue testing machine, developed by [Brincker, R. and J.D. Sørensen; 1990], and one used to control the DIP, see [Lyngbye, J. and R. Brincker; 1990].

The main advantages of DIP are: A more precise measuring of the crack length; short interruptions of the loading (5-10 seconds) during measuring and less resource demanding since, nobody has to survey the test.

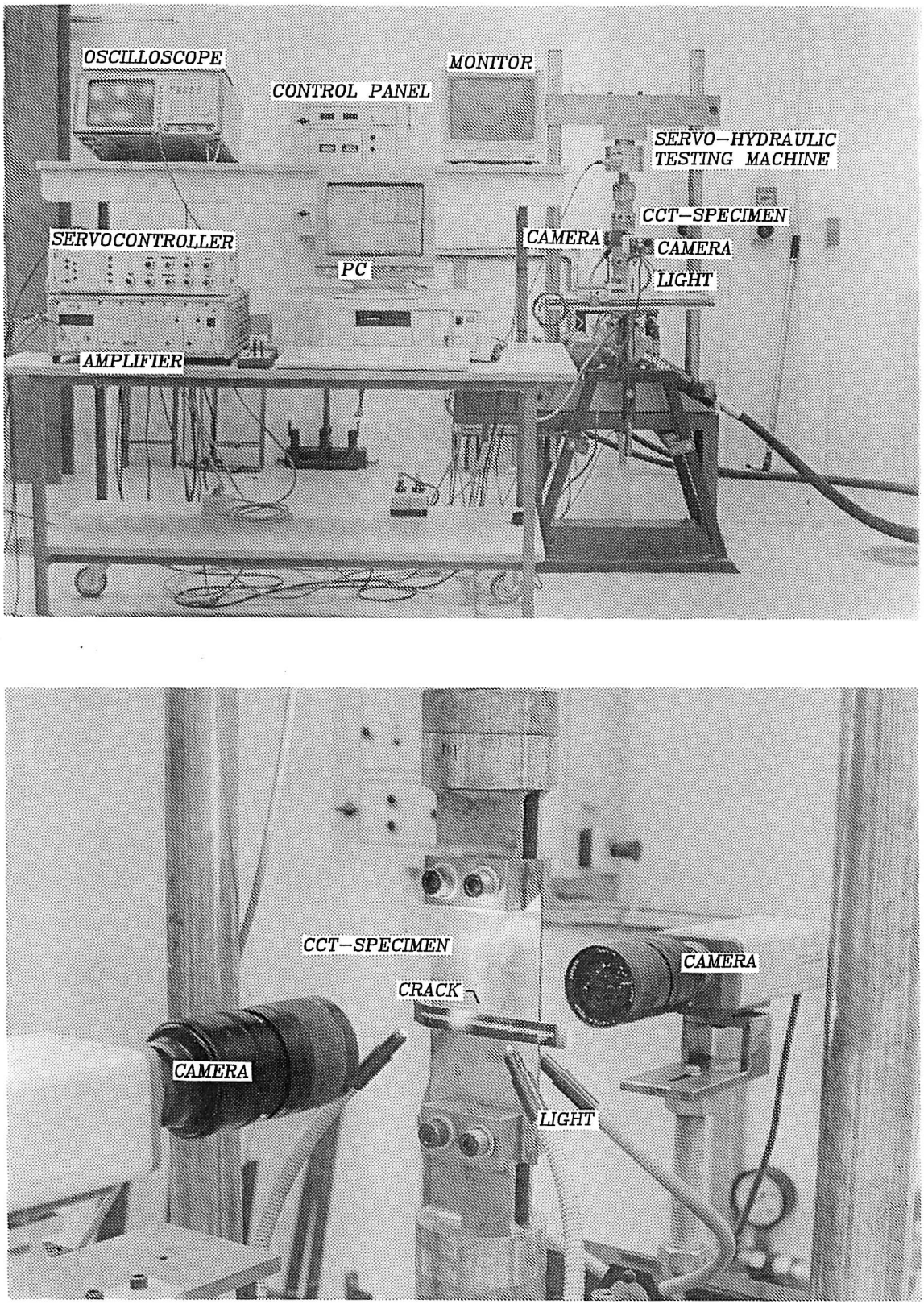

Figure 3.2: Test equipment for fatigue testing.

3.1 SN-Curve

In order to get an idea of the fatigue properties of mild steel given in table 1.1, an SN-curve is established in this section. Further, the SN-curve serves as a basis for the choice of stress range level in the fatigue crack growth tests described in section 3.2.

Determination of the structural resistance to fatigue can be obtained from an SN-curve, established by a series of tests carried out at different stress ranges. In each test, which is performed with CA-load, related values of the number of cycles to cause fracture, N_c, and stress range $\Delta\sigma$ are registered. In this illustration it is traditional to denote the number of cycles to cause fracture N and the stress range S. Minimum 8-12 corresponding SN-values are required for drawing an SN-curve.

If the number of stress cycles at a certain point of the structure is known, the maximum permissible stress range for that point, $\Delta\sigma_c$, can be obtained from the SN-curve. On the other hand, if the actual stress range is known then the maximum permissible number of cycles, N_c, can be found.

On the basis of the SN-curve, it is possible to estimate the damage accumulation e.g. by use of the Palmgren-Miner rule in which it is assumed that the damage accumulation depends solely on the stress variation, see e.g. [Leve, H.L.; 1969].

The tests used for establishing the SN-curve are outlined in table 3.3. The test frequency was 30 Hz.

TEST SPECIMEN	ΔP [kN]	P_m [kN]	$P_{\min}$ [kN]	$P_{\max}$ [kN]
36, 64, 99	35	18	0.5	35.5
2, 26, 61	30	15.5	0.5	30.5
19, 31, 49	25	13	0.5	25.5
13, 82, 93	20	10.5	0.5	20.5
7, 43, 75	15	8	0.5	15.5

Table 3.3: Review of constant-amplitude load fatigue tests, used to establish the SN-curve.
Load range $\Delta P = P_{\max} - P_{\min}$, mean load $P_m = \frac{1}{2}(P_{\max} + P_{\min})$, $P_{\max}$ = maximum load and $P_{\min}$ = minimum load.

In each test, coherent values of the number of cycles to fracture N_c and the stress range $\Delta\sigma$ were registered, see table 3.4. Further, the fracture crack length was measured using a slide gauge.

TEST SPECIMEN	$\Delta\sigma$ [MPa]	N_c	a_c [mm]
36	175	85004	12.35
64	175	87133	13.15
99	175	95493	11.85
2	150	165869	16.35
61	150	169409	17.40
26	150	173926	16.75
31	125	341537	21.40
19	125	365854	20.95
49	125	366508	20.70
13	100	745761	24.85
82	100	785261	24.75
93	100	787116	24.65
43	75	2329197	29.10
75	75	4756346	29.20
7	75	5325000	28.70

Table 3.4: Results of the fatigue tests in table 3.3.
$\Delta\sigma$ = stress range. N_c = number of cycles to fracture. a_c = fracture crack length.

On the basis of these values the SN-curve shown in figure 3.5 is drawn.

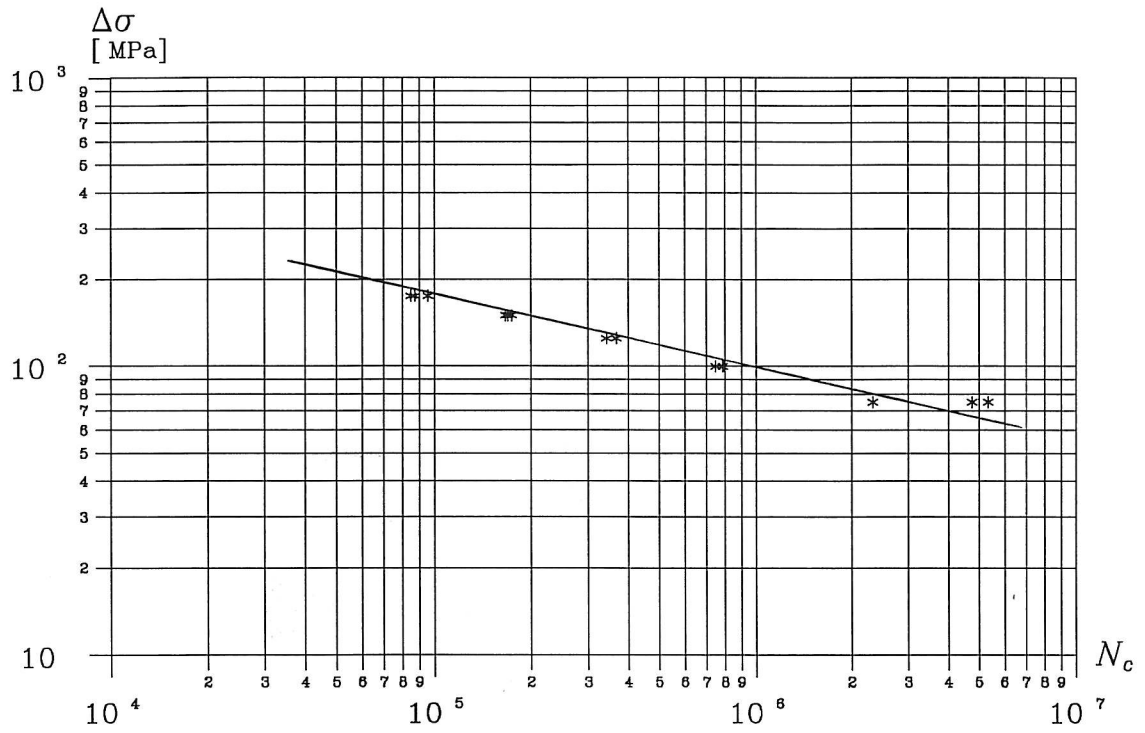

Figure 3.5: SN-curve for CCT-specimens of mild steel.
N_c = number of load cycles to cause fracture. $\Delta\sigma$ = stress range.

From table 3.4 and figure 3.5 it is seen that a small stress range results in a large critical crack length, which leaves the possibility of a large number of measurements, but on the other hand a long time of testing. In contrast, a large stress range gives a smaller critical crack length and thus the possibility of a fewer number of measurements, but a short time of testing.

According to figure 3.5, a threshold value of the stress range seems to appear so that stress ranges below this value do not cause fatigue. This corresponds to the loads applied to the structure being insufficient to create the necessary plastic deformation to advance the crack. Even though the threshold value is not well defined it can, as a general rule, be assumed that the value has not been reached if the stress range does not cause fracture after 2-5 million cycles or even more, [Gurney, T.R.; 1979, p.14]. The uncertainty of the threshold value is due to the extensive time consumption which is necessary for its determination.

The stress range used in the fatigue crack growth tests is chosen as $\Delta\sigma = 125$ MPa at the mean stress level $\sigma_m = 65$ MPa ($\Delta P = 25$ kN and $P_m = 13$ kN). This stress range allows a reasonable number of crack length measurements and a reasonable time of testing (≈ 4 hours at a frequency of 30 Hz). The fatigue crack growth tests are described in section 3.2.

3.2 Fatigue Crack Growth Curves

The fatigue crack growth tests described in theis section were performed with constant-amplitude load (CA-load). As mentioned in section 3.1, the stress range $\Delta\sigma = 125$ MPa with mean stress $\sigma_m = 65$ MPa.

In each test the number of load cycles and the crack length (N, a) were recorded for fixed values of δN by use of the DIP technique (Digital Image Processing).

It would be more convenient to measure for fixed values of δa and not δN, but so far this is not possible with the DIP technique and thus, measurements with fixed δa values would have required manual performance of the tests. The latter solution includes several disadvantages e.g. less accuracy and larger resources in the form of working hours. The problem was solved by interpolating the (N, a)-values corresponding to fixed values of δa.

The (N, a)-curves are shown in figure 3.6 where $(N_0, a_0) = (0, 3.0 \text{ mm})$ for all curves.

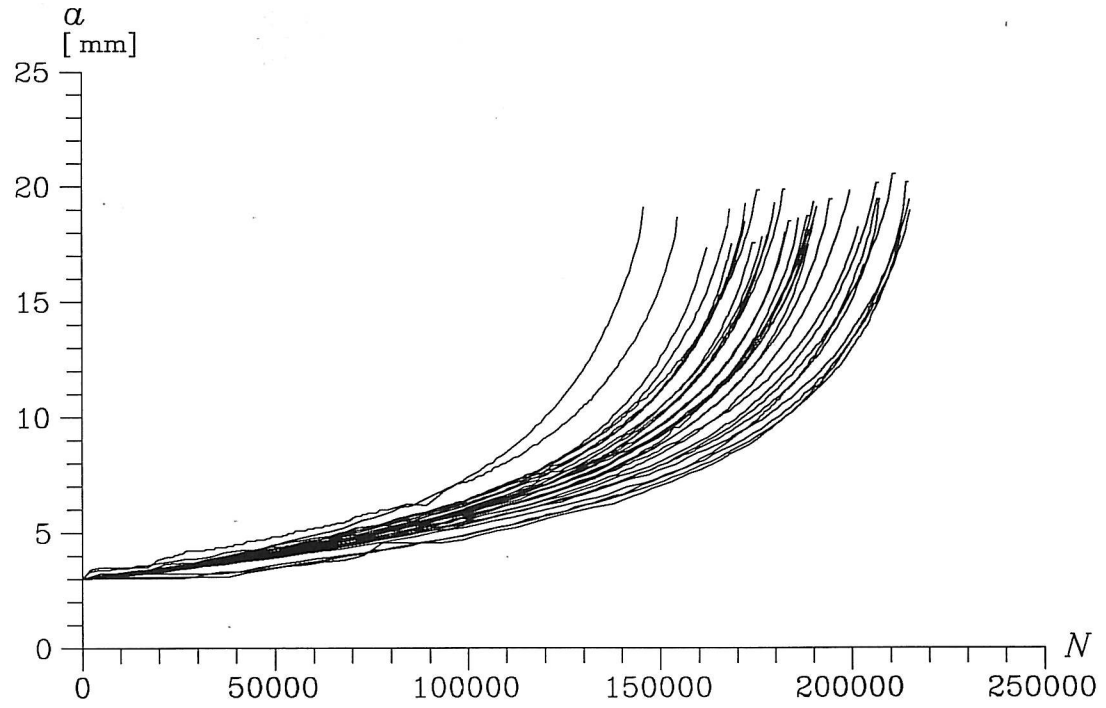

Figure 3.6: (N, a)-curves for CA-load tests performed in the spring of 1990. All 34 tests were performed with $\Delta P = 25$ kN. Material parameters are given in table 1.1.
N = number of load cycles, a = crack length.

From figure 3.6 it is seen that the curves have the same form and that they are characterized by a smooth progress. The approach to a vertical line for large a-values would have been more significant if the failure crack length a_f was obtained for larger crack lengths, i.e. for $a \geq 0.5\, a_{\max}$, where $a_{\max} = 0.5\, b = 40$ mm (see figure 3.1). But, the measuring method is very sensitive to changes in the surface of

the specimen which makes its impossible to measure when the plastic deformations become too large.

Further, it is seen that a large initial crack growth rate results in a small number of cycles to failure, N_f, and vice versa, and that there is a small tendency towards getting larger values of a_f for increasing N_f.

The material parameters C and m are determined on the basis of the (N, a)-data by calculating the crack growth rate (da/dN) and the stress intensity factor range (ΔK).

The stress intensity factor range for a finite CCT-specimen is given as, [ASTM E647-83].

$$\Delta K = \Delta\sigma\sqrt{\pi\, a \sec\left(\frac{\pi\, a}{b}\right)} \tag{3.1}$$

where the applied stress range $\Delta\sigma = 125$ MPa, the width of the specimen $b = 80$ mm and $a =$ the crack length.

The crack growth rate (da/dN) is found as the secant between two adjacent (N, a)-values, i.e.

$$\left(\frac{da}{dN}\right)_{a=\frac{1}{2}(a_i+a_{i+1})} = \frac{a_{i+1} - a_i}{N_{i+1} - N_i} \tag{3.2}$$

The CCT-specimen shown in figure 3.1 is designed so plane stress state occurs during the entire experiment. Evaluation of the extent of the plastic zone (r_y) in front of the crack tip is based on Irwin's second approximation, see e.g. [Hellan, K.; 1985, p.18],

$$r_y = \frac{1}{\pi}\left(\frac{K_I}{f_y}\right)^2 = \left(\frac{\sigma_{\max}}{f_y}\right)^2 a \sec\left(\frac{\pi a}{b}\right) \tag{3.3}$$

where (3.1) is used for the maximum stress intensity factor for K_I.

Insertion of $f_y = 266$ MPa (see table 2.3), $\sigma_{\max} = 127.5$ MPa, $w = 80$ mm and the initial crack length $a_0 = 3.0$ mm and the failure length $a_f = 17.5$ mm results in

$$r_y = \begin{cases} 0.69\,\text{mm} & \text{for } a_0 = 3.0 \text{ mm} \\ 4.02\,\text{mm} & \text{for } a_f = 17.5 \text{ mm} \end{cases}$$

Since the extent of the plastic zone is $\approx 20\%$ of the crack length it might be necessary to replace the crack length a by an effective crack length. According to [Gurney, T.R.; 1979, pp.44-47] the correction for crack tip plasticity should be a fraction of the plastic zone r_y, e.g. half the value of r_y. Thus, the effective crack length is given as

$$a_{\text{eff}} = a + \tfrac{1}{2} r_y \tag{3.4}$$

Introducing (3.4) into (3.1), the stress intensity factor range becomes

$$\Delta K = \Delta\sigma \sqrt{\pi\, a_{\text{eff}} \sec\left(\frac{\pi\, a_{\text{eff}}}{b}\right)} \tag{3.5}$$

and in (3.2), the crack growth rate is

$$\left(\frac{da}{dN}\right)_{a=\frac{1}{2}(a_{\text{eff},i}+a_{\text{eff},i+1})} = \frac{a_{\text{eff},i+1} - a_{\text{eff},i}}{N_{i+1} - N_i} \tag{3.6}$$

On the basis of (3.1)-(3.2) or (3.5)-(3.6), the material parameters C and m can be found by linear regression analysis bearing in mind that if $(\Delta K, da/dN)$ is represented in a double logarithmic scale, see figure 3.5, C and m can be found as the intersection with the ordinate axis and as the slope of the straight line, respectively. Thus,

$$\log(\frac{da}{dN}) = \log C + m \log(\Delta K) \tag{3.7}$$

Both the results from (3.1)-(3.2) and (3.5)-(3.6) are used.

The linear regression analysis gives the results in table 3.7.

		(3.1)-(3.2)	(3.5)-(3.6)
$\log C$	$[\text{mm}/(\text{MPa}\sqrt{\text{m}})^m]$	-8.60076	-8.53291
C	$[\text{mm}/(\text{MPa}\sqrt{\text{m}})^m]$	$2.5075 \cdot 10^{-9}$	$2.9315 \cdot 10^{-9}$
$S_{\log C}$	$[\text{mm}/(\text{MPa}\sqrt{\text{m}})^m]$	0.019	0.018
m		3.486	3.400
S_m		0.014	0.013

Table 3.7: Values of the material parameters C and m found from experimental data by the linear regression analysis. Further, the standard deviations of $\log C$ and m are given.

It is seen that almost the same results for C and m are obtained no matter which of a or a_{eff} is used. Further, only small deviations are found, which means that (3.7) gives a good description of the data. The following calculations are therefore based on the crack length a, which is simpler than using the effective crack length.

In order to calculate the statistical properties of the (N, a)-curves, the data are transformed into (N, a)-data for fixed values of a, $a = a_0 + \delta a$, where $a_0 = 3.0$ mm,

$\delta a = 0.1$ mm and $a \in [3.0 \ ; \ 17.5]$mm. The transformation is performed by linear interpolation between the two adjacent values of a, one smaller and one greater than the desired a value. The corresponding N value is found in a similar manner.

All the following analyses are based on these (N, a)-data.

3.3 Statistical Analysis of the Fatigue Crack Growth Data

The statistical properties of the fatigue crack growth data from the CA-load tests in section 3.2 are given in the present section.

The statistical values, i.e. the mean value, the standard deviation and the probability density of the number of cycles applied in each crack state to reach the successive crack state and of the total number of cycles applied to reach a crack state, are determined as

$$\overline{\delta N}_j = \frac{1}{n} \sum_{i=1}^{n} (\delta N_j)_i \tag{3.8}$$

$$\mathrm{S}_{\delta N_j} = \left[\frac{1}{n-1} \sum_{i=1}^{n} ((\delta N_j)_i - \overline{\delta N}_j)^2 \right]^{\frac{1}{2}} \tag{3.9}$$

$$\mathrm{Q}_{\delta N_j} = \sum_{i=1}^{n} (\delta N_j | \delta N_j \in]k \cdot 250; (k+1) \cdot 250]) \tag{3.10}$$

$$\overline{N}_j = \frac{1}{n} \sum_{i=1}^{n} (N_j)_i \tag{3.11}$$

$$\mathrm{S}_{N_j} = \left[\frac{1}{n-1} \sum_{i=1}^{n} ((N_j)_i - \overline{N}_j)^2 \right]^{\frac{1}{2}} \tag{3.12}$$

$$\mathrm{Q}_{N_j} = \sum_{i=1}^{n} (N_j | N_j \in]k \cdot 10000; (k+1) \cdot 10000]) \tag{3.13}$$

Further, the autocovariance of the crack growth rate (da/dN) is determined as

$$\mathrm{C}_{(\frac{da}{dN})_j}(t_1, t_2) = \frac{1}{n} \sum_{i=1}^{n} \left[\mathrm{C}_{(\frac{da}{dN})_j}(t_1, t_2) \right]_i \tag{3.14}$$

where

$$\left[C_{\left(\frac{da}{dN}\right)_j}(t_1,t_2)\right]_i = \left\{E\left[\left(\frac{da}{dN}(t_1)\right)_j \cdot \left(\frac{da}{dN}(t_2)\right)_j\right] - E\left[\left(\frac{da}{dN}(t_1)\right)_j\right] \cdot E\left[\left(\frac{da}{dN}(t_2)\right)_j\right]\right\}_i \quad (3.15)$$

and where

i	=	$1,2,\ldots,n$
j	=	$0,1,2,\ldots,nn$
k	=	$0,1,2,\ldots,39$
n	=	number of crack growth tests
nn	=	number of crack states
δN_j	=	number of load cycles applied at the crack state j
$\overline{\delta N}_j$	=	mean value of the number of load cycles applied at the crack state j
$S_{\delta N_j}$	=	standard deviation of the number of load cycles applied at crack state j
$Q_{\delta N_j}$	=	histogram of the number of load cycles applied at crack state j
N_j	=	total number of load cycles applied to reach the crack state j
$\overline{N}_j$	=	mean value of the total number of load cycles applied to reach the crack state j
S_{N_j}	=	standard deviation of the total number of load cycles applied to reach the crack state j
Q_{N_j}	=	histogram of total number of load cycles applied to reach the crack state j
$C_{\left(\frac{da}{dN}\right)_j}$	=	autocovariance of crack growth rate in state j
t_1, t_2	=	time instants 1 and 2, e.g. crack state 1 and 2

The results are shown in figures 3.8-3.16 for $n = 34$ and $nn = 145$.

The histograms in figure 3.10 are shown for the crack lengths $a_0 = 3.0$ mm, $a_{72} = 10.2$ mm and $a_{144} = 17.4$ mm, corresponding to the first, middle and final crack states for which the number of load cycles applied at a crack state is measured. The corresponding crack lengths for which the total number of cycles is measured are $a_1 = 3.1$ mm, $a_{73} = 10.3$ mm and $a_{145} = 17.5$ mm. The histograms for these crack lengths are illustrated in figure 3.13.

Each interval I_k in the histograms consists of a number of load cycles - 250 for δN_j and 10000 for N_j - distributed as $I_k =]k{\cdot}250\ ;\ (k+1){\cdot}250]$ cycles and $I_k =]k{\cdot}10000\ ;\ (k+1){\cdot}10000]$ cycles, respectively. $k = 0,1,2,\ldots,39$.

The autocovariane of da/dN is shown for the same crack lengths as in figure 3.10, i.e. $a_0 = 3.0$ mm, $a_{72} = 10.2$ mm and $a_{144} = 17.4$ mm, see figures 3.14-3.16.

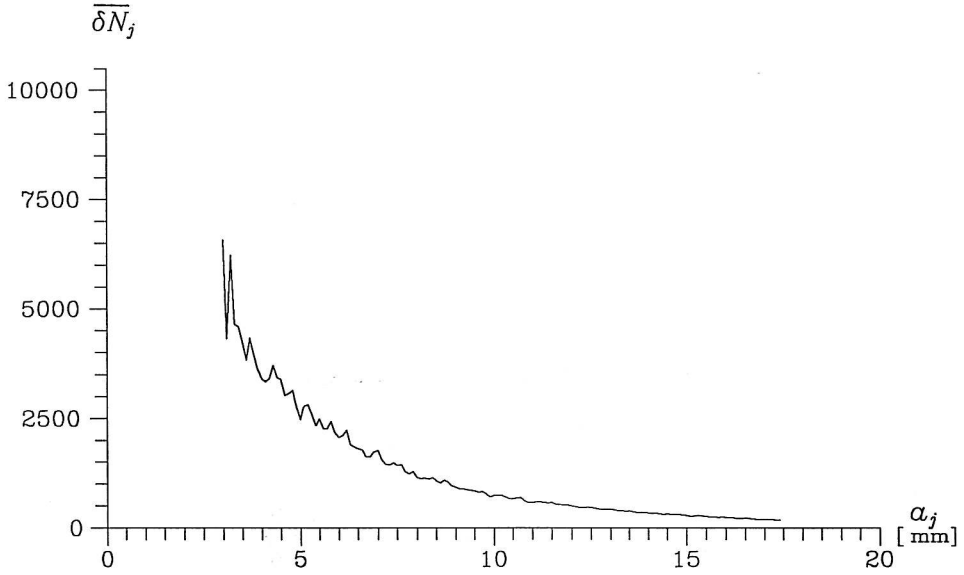

Figure 3.8: Mean value of the number of load cycles ($\overline{\delta N_j}$) applied at each crack state (a_j) for CA-load tests.
$j = 0, 1, 2, \ldots, 144$, $a_0 = 3.0$ mm and $a_{144} = 17.4$ mm.

Figure 3.8 shows that the mean number of load cycles $\overline{\delta N_j}$ applied at the crack state a_j decreases with increasing crack length, which could be expected because the crack growth rate increases during the lifetime.

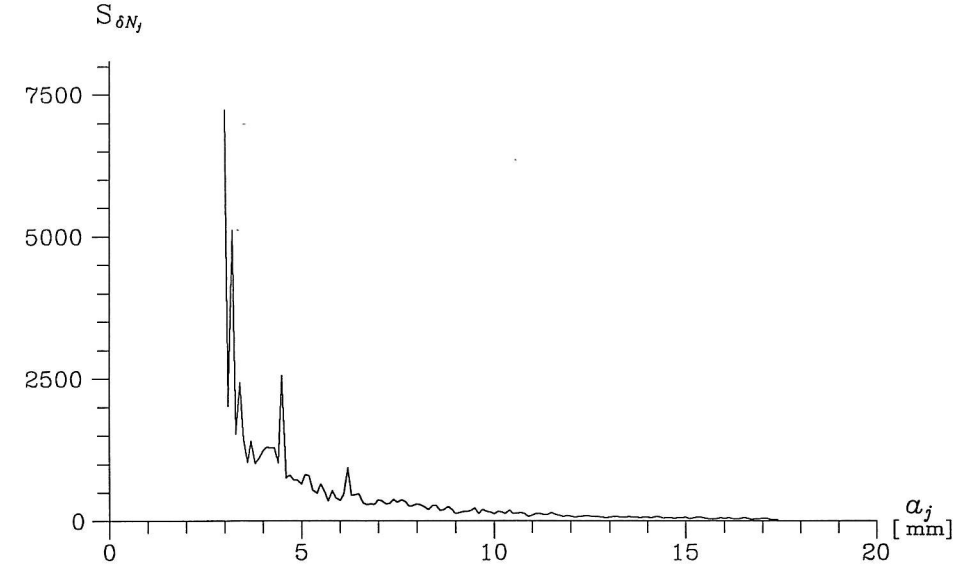

Figure 3.9: Standard deviation of the number of load cycles ($S_{\delta N_j}$) applied at each crack state (a_j), for CA-load tests.
$j = 0, 1, 2, \ldots, 144$, $a_0 = 3.0$ mm and $a_{144} = 17.4$ mm.

The standard deviation of the number of load cycles $S_{\delta N_j}$ applied at a crack state a_j decreases with increasing crack length, see figure 3.9. The scatter in the standard deviation is seen to be large for small crack lengths ($a \leq 5$ mm), whereas it is small for large crack lengths.

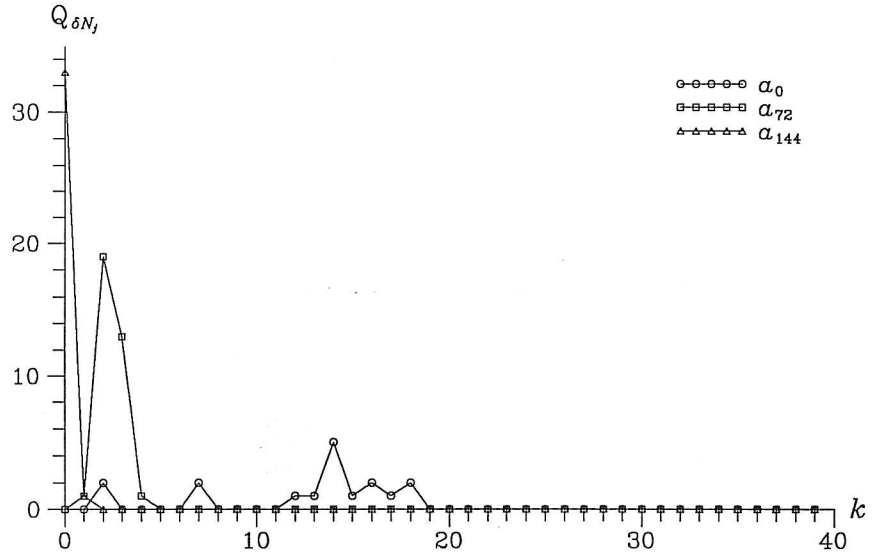

Figure 3.10: Histogram of the number of load cycles ($Q_{\delta N_0}$), ($Q_{\delta N_{72}}$) and ($Q_{\delta N_{144}}$) applied at the crack state $a_0 = 3.0$ mm, $a_{72} = 10.2$ mm and $a_{144} = 17.4$ mm, respectively.
$I_k =]k{\cdot}250\ ;\ (k+1){\cdot}250]$ cycles, $k = 0, 1, 2, \ldots, 39$.

From figure 3.10 it is seen that the histogram $Q_{\delta N_0}$ is uniformly distributed over all intervals.

The decrease in the standard deviation of δN_j is reflected in the probability density $Q_{\delta N_{72}}$. Thus, only 4 intervals (I_1 to I_4, i.e. $\delta N_{72} \in]250\ ;\ 1250]$ cycles) are included.

No matter how many cycles have been applied to reach crack state $a_{144} = 17.4$ mm, almost the same number of cycles is required to reach the failure state. This is seen in figure 3.10 in which $Q_{\delta N_{144}}$ is concentrated on 2 intervals. Thus, $\delta N_{144} \in]0\ ;\ 500]$ cycles.

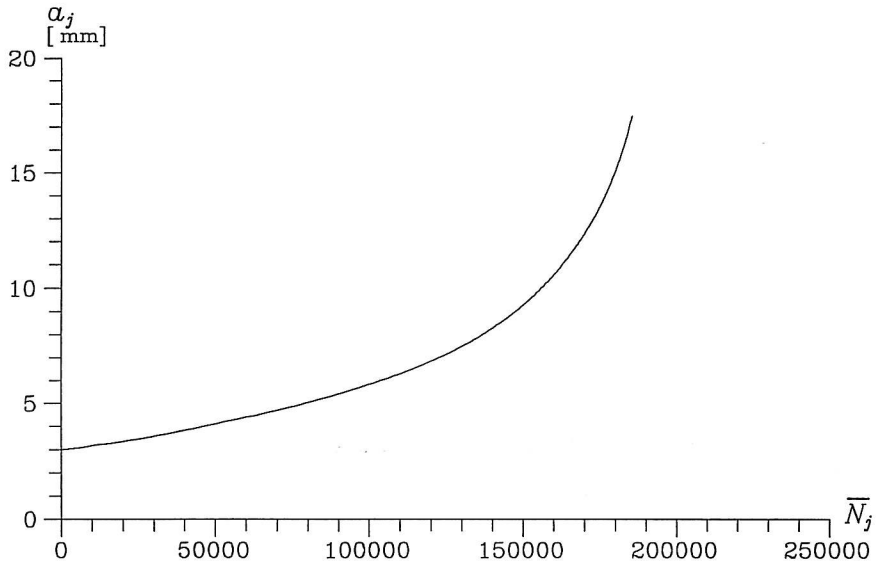

Figure 3.11: Mean value of the number of load cycles ($\overline{N}_j$) applied to reach the crack state (a_j), for CA-load tests.
$j = 0, 1, 2, \ldots, 145$, $a_0 = 3.0$ mm and $a_{145} = 17.5$ mm.

The mean number of load cycles $\overline{N}_j$ applied to reach a crack state a_j has a smooth, non-decreasing progress, see figure 3.11, and the number of cycles to cause failure N_f is 185353 cycles.

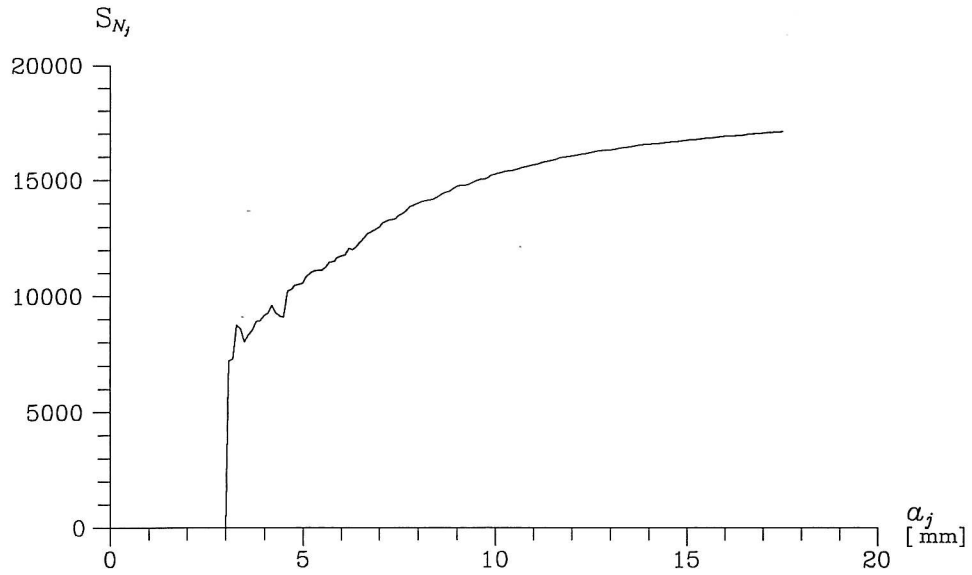

Figure 3.12: Standard deviation of the number of load cycles (S_{N_j}) applied to reach the crack state (a_j), for CA-load tests.
$j = 0, 1, 2, \ldots, 145$, $a_0 = 3.0$ mm and $a_{145} = 17.5$ mm.

It is seen in figure 3.12 that the standard deviation of the number of load cycles S_{N_j} applied to reach the crack state a_j increases with increasing crack length. The rate

of increase is largest for small crack lengths ($a < 7$ mm) after which the standard deviation slowly increases towards a constant value of ≈ 17000. The relative deviation is $\approx 9\%$.

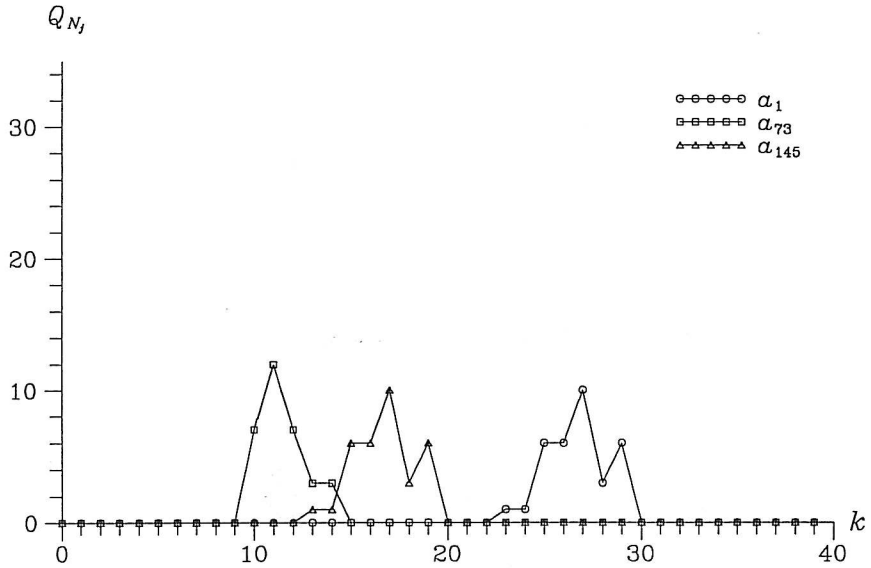

Figure 3.13: Histogram of the number of load cycles (Q_{N_1}), ($Q_{N_{73}}$) and ($Q_{N_{145}}$) applied to reach the crack state $a_1 = 3.1$ mm, $a_{73} = 10.3$ mm and $a_{145} = 17.5$ mm, respectively.
$I_k =]k{\cdot}10000\ ;\ (k+1){\cdot}10000]$ cycles, $k = 0, 1, 2, \ldots, 39$.

The distribution of the histogram Q_{N_1} in figure 3.13 shows that only one interval is included, i.e. $N_1 \in]0\ ;\ 10000]$ cycles.

Due to the larger scatter at crack state $a_{73} = 10.3$ mm more intervals are included. The CA-load tests are distributed over I_{12} to I_{18}, i.e. $N_{73} \in]120000\ ;\ 190000]$ cycles.

The same tendency is found for $Q_{N_{145}}$ in figure 3.13, but with the intervals I_{14} to I_{22}, i.e. $N_{145} \in]140000\ ;\ 230000]$ cycles. The overlap of intervals for N_{73} and $N_f = N_{145}$ corresponds to N_{73} being larger than N_f for some tests.

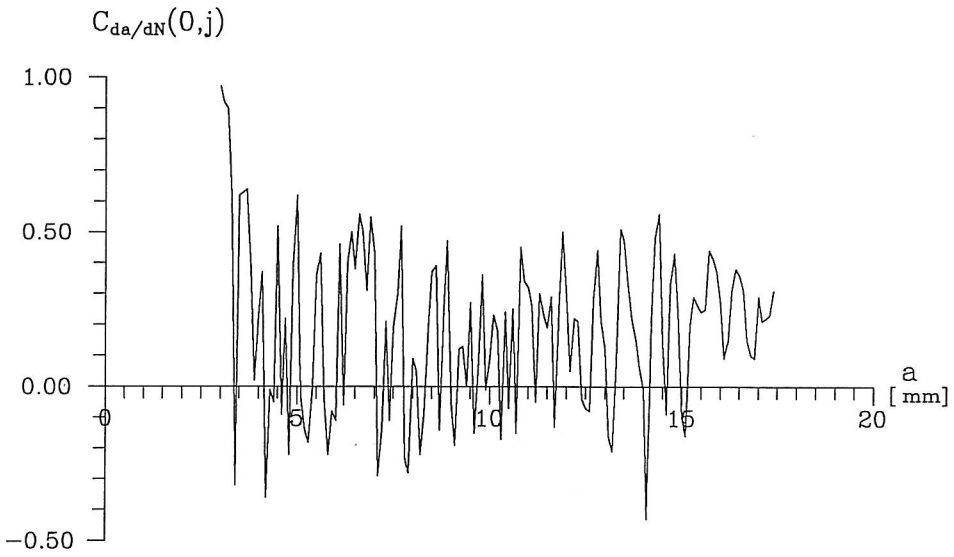

Figure 3.14: Autocovariance of the crack growth rate in crack state $a_0 = 3.0$ mm for CA-load tests.
$j = 0, 1, 2, \ldots, 144$.

As seen in figure 3.14 the autocovariance $C_{da/dN}(0, j)$ is concentrated within the interval [-0.25 ; 0.55] which indicates that the crack growth rate throughout the lifetime is greatly dependent on the initial crack growth rate. Further, it seems that the mean value is almost constantly (≈ 0.15).

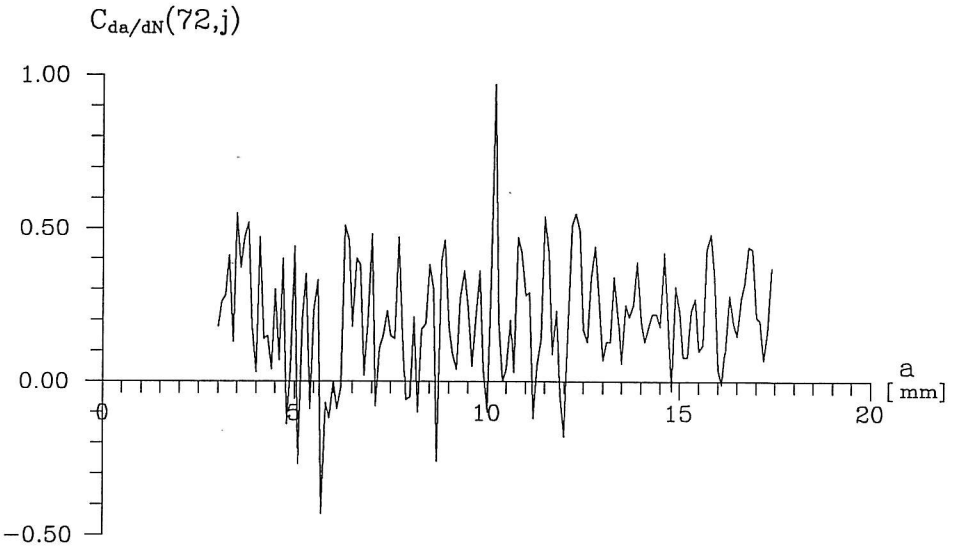

Figure 3.15: Autocovariance of the crack growth rate in crack state $a_{72} = 10.2$ mm for CA-load tests.
$j = 0, 1, 2, \ldots, 144$.

In figure 3.15 the same tendency as in figure 3.14 is seen. Thus, the autocovariance

$C_{da/dN}(72, j)$ is concentrated within the interval [-0.15 ; 0.50] with constant mean value (≈ 0.20) meaning that the crack growth rate obtained before crack state $a_{72} = 10.2$ mm influences the crack growth rate in this crack state which again influences the crack growth rate after crack state $a_{72} = 10.2$ mm.

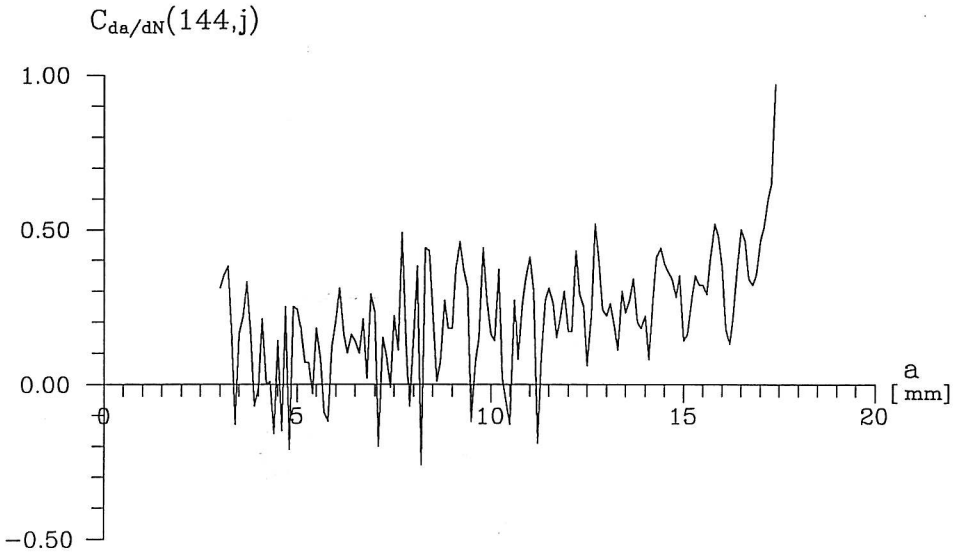

Figure 3.16: Autocovariance of the crack growth rate in crack state $a_{144} = 17.4$ mm for CA-load tests.
$j = 0, 1, 2, \ldots, 144$.

The autocovariance $C_{da/dN}(144, j)$ shown in figure 3.16 differs from the ones in figures 3.14 and 3.15 since the mean value increases for increasing crack length. Thus, $C_{da/dN}(144, j)$ starts with values in the interval [-0.20 : 0.25] ending with values in the interval [0.15 ; 0.55].

The curves shown in figures 3.8-3.16 form the basis of comparison of the CA-load tests and the test of the FMF-model, see [Gansted, L., R. Brincker and L. Pilegaard Hansen; 1994].

4. CONCLUSIONS

The purpose of the present paper was to determine the fatigue properties of mild steel.

Firstly, the traditional material parameters were determined in static tests, see chapter 2.

Secondly, tests with time-varying load with constant-amplitude and different stress ranges were performed in order to establish an SN-curve, see section 3.1.

Based on these results a series of fatigue crack growth curves was established experi-

mentally in identical tests (same stress range), see section 3.2. The curves show great similarity and form the basis for caluculating the Paris constants C and m. Further, the (N, a)-data serve as reference data for a fatigue model described in [Gansted, L., R. Brincker and L.Pilegaard Hansen; 1994].

The statistical values of the data in the form of the mean value, the standard deviation and the probability density of the number of cycles applied in each crack state to reach the successive crack state and of the total number of cycles applied to reach a crack state are given in section 3.3. Further, histograms and autocovariances are given for three different crack lengths.

REFERENCES

[ASTM STP E647-83; 1985]
"Standard Test Method for Constant-Load-Amplitude Fatigue Crack Growth Rates Above 10^{-8} m/cycle"
1985 Annual Book of ASTM Standards Volume 03.01, pp.739-759
American Society for Testing and Materials

[Brincker, R. and J. D. Sørensen; 1990]
"High-Speed Stochastic Fatigue Testing"
Experimental Mechanics, Vol., No., pp.4-9
Society of Experimental Mechanics

[Gansted, L., R. Brincker and L.Pilegaard Hansen; 1991]
"Fracture Mechanical Markov Chain Crack Growth Model"
Engineering Fracture Mechanics, Vol.38, N0.6, pp.475-489
Pergamon Press plc.

[Gansted, L., R. Brincker and L.Pilegaard Hansen; 1994]
"The Fracture Mechanical Markov Chain Fatigue Model Compared with Empirical Data"
Fracture and Dynamics, Paper
University of Aalborg

[Gurney, T.R.; 1979]
"Fatigue of Welded Structures"
Cambridge University Press, 2nd edition

[Hellan, K.; 1985]
"Introduction to Fracture Mechanics"
McGraw-Hill Book Co. - International Student Edition

[Leve, H.L.; 1969]
"Cumulative Damage Theories"
Metal Fatigue: Theory and Design, pp.170-203
John Wiley & Sons, Inc.

[Lyngbye, J. and R. Brincker; 1990]
"Crack Length Detection by Digital Image Processing"
Fracture and Dynamics, Paper No.23, June 1990
ISSN 0902-7513R9018
University of Aalborg, Denmark

SYMBOLS

a	=	crack length
a_0	=	initial crack length
a_c	=	critical crack length
a_{eff}	=	effective crack length
a_f	=	failure crack length
$a_{\max}$	=	maximum crack length
δa	=	crack length increase
w	=	width
C	=	material constant
C[.]	=	autocovariance of random variable
da	=	crack length increase
dN	=	increase in number of cycles
E	=	Young's modulus
f_u	=	ultimate stress
f_y	=	yield stress
I_k	=	interval of histogram
K_I	=	stress intensity factor in mode I
ΔK	=	stress intensity factor range
l_0	=	undeformed length
l_i	=	initial length between strengthen clamps
l_u	=	deformed length
m	=	material constant
N	=	number of cycles
$\overline{N}$	=	mean value of number of cycles
N_0	=	initial number of cycles
N_c	=	number of cycles to cause fracture
N_f	=	number of cycles to cause failure
δN	=	increase in number of cycles
$\overline{\delta N}$	=	mean value of increase in number of cycles
P	=	load
P_m	=	mean load
P_u	=	load at which fracture takes place
P_x	=	force in direction x
P_y	=	load at which yielding takes place
$P_{\max}$	=	maximum load
$P_{\min}$	=	minimum load
ΔP	=	load range
Q[.]	=	histogram of random variable
r_y	=	plastic zone size
S	=	stress range
S[.]	=	standard deviation of random variable
t	=	thickness
t_i	=	time moment, $i = 1, 2$

ϵ_i = strain component in Cartesian coordinate system ($i = x, y$)
ϵ_u = ultimate strain
ν = Poisson's ratio
σ_i = stress component in Cartesian coordinate system ($i = x, y$)
σ_m = mean stress
$\sigma_{\max}$ = maximum stress
$\Delta\sigma$ = stress range
$\Delta\sigma_c$ = critical stress range

FRACTURE AND DYNAMICS PAPERS

PAPER NO. 18: Jakob Laigaard Jensen, Rune Brincker & Anders Rytter: *Uncertainty of Modal Parameters Estimated by ARMA Models.* ISSN 0902-7513 R9006.

PAPER NO. 19: Rune Brincker: *Crack Tip Parameters for Growing Cracks in Linear Viscoelastic Materials.* ISSN 0902-7513 R9007.

PAPER NO. 20: Rune Brincker, Jakob L. Jensen & Steen Krenk: *Spectral Estimation by the Random Dec Technique.* ISSN 0902-7513 R9008.

PAPER NO. 21: P. H. Kirkegaard, J. D. Sørensen & Rune Brincker: *Optimization of Measurements on Dynamically Sensitive Structures Using a Reliability Approach.* ISSN 0902-7513 R9009.

PAPER NO. 22: Jakob Laigaard Jensen: *System Identification of Offshore Platforms.* ISSN 0902-7513 R9011.

PAPER NO. 23: Janus Lyngbye & Rune Brincker: *Crack Length Detection by Digital Image Processing.* ISSN 0902-7513 R9018.

PAPER NO 24: Jens Peder Ulfkjær, Rune Brinker & Steen Krenk: *Analytical Model for Complete Moment-Rotation Curves of Concrete Beams in bending.* ISSN 0902-7513 R9021.

PAPER NO 25: Leo Thesbjerg: *Active Vibration Control of Civil Engineering Structures under Earthquake Excitation.* ISSN 0902-7513 R9027.

PAPER NO. 26: Rune Brincker, Steen Krenk & Jakob Laigaard Jensen: *Estimation of correlation Functions by the Random Dec Technique.* ISSN 0902-7513 R9028.

PAPER NO. 27: Jakob Laigaard Jensen, Poul Henning Kirkegaard & Rune Brincker: *Model and Wave Load Identification by ARMA Calibration.* ISSN 0902-7513 R9035.

PAPER NO. 28: Rune Brincker, Steen Krenk & Jakob Laigaard Jensen: *Estimation of Correlation Functions by the Random Decrement Technique.* ISSN 0902-7513 R9041.

PAPER NO. 29: Poul Henning Kirkegaard, John D. Sørensen & Rune Brincker: *Optimal Design of Measurement Programs for the Parameter Identification of Dynamic Systems.* ISSN 0902-7513 R9103.

PAPER NO. 30: L. Gansted & N. B. Sørensen: *Introduction to Fatigue and Fracture Mechanics.* ISSN 0902-7513 R9104.

PAPER NO. 31: R. Brincker, A. Rytter & S. Krenk: *Non-Parametric Estimation of Correlation Functions.* ISSN 0902-7513 R9120.

PAPER NO. 32: R. Brincker, P. H. Kirkegaard & A. Rytter: *Identification of System Parameters by the Random Decrement Technique.* ISSN 0902-7513 R9121.

PAPER NO. 33: A. Rytter, R. Brincker & L. Pilegaard Hansen: *Detection of Fatigue Damage in a Steel Member.* ISSN 0902-7513 R9138.

FRACTURE AND DYNAMICS PAPERS

PAPER NO. 34: J. P. Ulfkjær, S. Krenk & R. Brincker: *Analytical Model for Fictitious Crack Propagation in Concrete Beams.* ISSN 0902-7513 R9206.

PAPER NO. 35: J. Lyngbye: *Applications of Digital Image Analysis in Experimental Mechanics.* Ph.D.-Thesis. ISSN 0902-7513 R9227.

PAPER NO. 36: J. P. Ulfkjær & R. Brincker: *Indirect Determination of the $\sigma - w$ Relation of HSC Through Three-Point Bending.* ISSN 0902-7513 R9229.

PAPER NO. 37: A. Rytter, R. Brincker & P. H. Kirkegaard: *An Experimental Study of the Modal Parameters of a Damaged Cantilever.* ISSN 0902-7513 R9230.

PAPER NO. 38: P. H. Kirkegaard: *Cost Optimal System Identification Experiment Design.* ISSN 0902-7513 R9237.

PAPER NO. 39: P. H. Kirkegaard: *Optimal Selection of the Sampling Interval for Estimation of Modal Parameters by an ARMA-Model.* ISSN 0902-7513 R9238.

PAPER NO. 40: P. H. Kirkegaard & R. Brincker: *On the Optimal Location of Sensors for Parametric Identification of Linear Structural Systems.* ISSN 0902-7513 R9239.

PAPER NO. 41: P. H. Kirkegaard & A. Rytter: *Use of a Neural Network for Damage Detection and Location in a Steel Member.* ISSN 0902-7513 R9245

PAPER NO. 42: L. Gansted: *Analysis and Description of High-Cycle Stochastic Fatigue in Steel.* Ph.D.-Thesis. ISSN 0902-7513 R9135.

PAPER NO. 43: M. Krawczuk: *A New Finite Element for Static and Dynamic Analysis of Cracked Composite Beams.* ISSN 0902-7513 R9305.

PAPER NO. 44: A. Rytter: *Vibrational Based Inspection of Civil Engineering Structures.* Ph.D.-Thesis. ISSN 0902-7513 R9314.

PAPER NO. 45: P. H. Kirkegaard & A. Rytter: *An Experimental Study of the Modal Parameters of a Damaged Steel Mast.* ISSN 0902-7513 R9320.

PAPER NO. 46: P. H. Kirkegaard & A. Rytter: *An Experimental Study of a Steel Lattice Mast under Natural Excitation.* ISSN 0902-7513 R9326.

PAPER NO. 47: P. H. Kirkegaard & A. Rytter: *Use of Neural Networks for Damage Assessment in a Steel Mast.* ISSN 0902-7513 R9340.

PAPER NO. 48: R. Brincker, M. Demosthenous & G. C. Manos: *Estimation of the Coefficient of Restitution of Rocking Systems by the Random Decrement Technique.* ISSN 0902-7513 R9341.

PAPER NO. 49: L. Gansted: *Fatigue of Steel: Constant-Amplitude Load on CCT-Specimens.* ISSN 0902-7513 R9344.

Department of Building Technology and Structural Engineering
The University of Aalborg, Sohngaardsholmsvej 57, DK 9000 Aalborg
Telephone: 45 98 15 85 22 Telefax: 45 98 14 82 43